Received: 29 March 2021 | Revised: 2 June 2021 | Accepted: 18 August 2021

DOI: 10.1002/mp.15209

RESEARCH ARTICLE

MEDICAL PHYSICS

Dose calculation accuracy in particle therapy: Comparing carbon ions with protons

Sirinya Ruangchan[1,2] | **Hugo Palmans**[3,4] | **Barbara Knäusl**[1,3] | **Dietmar Georg**[1,3] | **Monika Clausen**[1]

[1] Department of Radiation Oncology, Medical University of Vienna, Vienna, Austria

[2] Department of Radiology, King Chulalongkorn Memorial Hospital, Bangkok, Thailand

[3] Division of Medical Physics, MedAustron Ion Therapy Center, Wiener Neustadt, Austria

[4] Medical Radiation Science, National Physical Laboratory, Teddington, UK

Correspondence
Monika Clausen, Department of Radiation Oncology, Medical University of Vienna, Währinger Gürtel 18-20, 1090 Wien, Austria.
Email: monika.clausen@meduniwien.ac.at

Abstract

Purpose: This work presents the validation of an analytical pencil beam dose calculation algorithm in a commercial treatment planning system (TPS) for carbon ions by measurements of dose distributions in heterogeneous phantom geometries. Additionally, a comparison study of carbon ions versus protons is performed considering current best solutions in commercial TPS.

Methods: All treatment plans were optimized and calculated using the RayStation TPS (RaySearch, Sweden). The dose distributions calculated with the TPS were compared with measurements using a 24-pinpoint ionization chamber array (T31015, PTW, Germany). Tissue-like inhomogeneities (bone, lung, and soft tissue) were embedded in water, while a target volume of 4 x 4 x 4 cm^3 was defined at two different depths behind the heterogeneities. In total, 10 different test cases, with and without range shifter as well as different air gaps, were investigated. Dose distributions inside as well as behind the target volume were evaluated.

Results: Inside the target volume, the mean dose difference between calculations and measurements, averaged over all test cases, was 1.6% for carbon ions. This compares well to the final agreement of 1.5% obtained in water at the commissioning stage of the TPS for carbon ions and is also within the clinically acceptable interval of 3%. The mean dose difference and maximal dose difference obtained outside the target area were 1.8% and 13.4%, respectively. The agreement of dose distributions for carbon ions in the target volumes was comparable or better to that between Monte Carlo (MC) dose calculations and measurements for protons. Percentage dose differences of more than 10% were present outside the target area behind bone–lung structures, where the carbon ion calculations systematically over predicted the dose. MC dose calculations for protons were superior to carbon ion beams outside the target volumes.

Conclusion: The pencil beam dose calculations for carbon ions in RayStation were found to be in good agreement with dosimetric measurements in heterogeneous geometries for points of interest located within the target. Large local discrepancies behind the target may contribute to incorrect dose predictions for organs at risk.

KEYWORDS
carbon ions, dose calculation algorithms, heterogeneous phantom, protons

This is an open access article under the terms of the Creative Commons Attribution-NonCommercial License, which permits use, distribution and reproduction in any medium, provided the original work is properly cited and is not used for commercial purposes.
© 2021 The Authors. *Medical Physics* published by Wiley Periodicals LLC on behalf of American Association of Physicists in Medicine

1 | INTRODUCTION

The physical characteristics of light ions have great potential to improve clinical outcomes in radiotherapy. Except protons, only carbon ions are currently applied clinically, with 13 centers in operation worldwide.[1] Helium ions are expected to be the next ions species being clinically explored.

The physical advantage of carbon ions over protons is their reduced lateral scattering leading to a sharp lateral dose fall-off around the target. While for protons no dose is deposited behind the Bragg peak, for carbon ions projectile fragments from nuclear interactions form a so-called fragmentation tail that contributes to dose deposition behind target structures.[2,3] Fluctuations in the energy loss of individual ions ("energy straggling") lead to Bragg peak broadening and range uncertainties. The energy straggling for protons is a factor 3.5 larger than for carbon ions, resulting for protons in a broader Bragg peak. For practical reasons so-called ripple filters are typically inserted into the carbon ion beam line to broaden the Bragg peak to some degree and reduce the number of energy layers required to generate uniform dose distributions within the target. Another important aspect of carbon ions is that they are densely ionizing, resulting in radiobiological advantage for hypoxic and radioresistant tumors[4,5] and which may even generate stronger immunological responses.[6] Clinical research in carbon ion therapy is in an early stage.[5] Even though there are treatment sites which have predisposition to benefit from carbon ions, clinical evidence is limited so far.[4,5,7] Better understanding of physical limitations and radiobiological effects of carbon ion beams is necessary to improve the clinical outcome of carbon ion therapy.

Dose calculation accuracy is an important aspect in radiation oncology and benchmarking of algorithms in the presence of heterogeneities that mimic clinical scenarios are commonly performed irrespective of the treatment technique.[8–14] At present, numerous commercial treatment planning systems (TPSs) are in use for proton therapy among the most widely used are RayStation (RaySearch Laboratories, Sweden), Eclipse (Varian Medical Systems), Pinnacle (Philips), and XiO (Elekta).[15] All of them provide analytical pencil beam (PB) algorithms and some also a Monte Carlo-based (MC) algorithm. The limitations of PB algorithms for protons have been extensively studied,[16] with well-known shortcomings for heterogeneities, especially for lung[17–19,27,28] and treatments with a range shifter.[17,20,21] These studies underlined the importance of upcoming Monte Carlo dose calculation for routine clinical treatment planning, particularly for scanned proton beams.[14,15,22] PB algorithms represent the current global standard for carbon ion therapy. Japanese centers use mainly the TPS XiO-N (ELEKTA and Mitsubishi Electric), while European centers use either the TPS Syngo RT planning (Siemens) or RayStation.[23] As far as the TPS RayStation is concerned, PB algorithms are implemented differently for proton and carbon ion beams. To handle large scattering effects in the presence of inhomogeneous boundaries parallel to the beam direction, PB modeling for protons divides the physical beamlet into 19 sub-spots. Calculations are subsequently carried out for all individual sub-beams.[24] The calculated range of individual sub-spots depends on the material its central axis passes through. In other words, in this step the respective materials are considered to be laterally infinite.[25] In contrast to protons, carbon beams can be well described by the Gaussian small angle approximation when traversing matter, and no sub-spot division of the beamlet is therefore introduced in the analytical PB model.[26] Even though the lateral scatter for carbon ion beams is small, the dose calculation performance might be, similarly to protons, challenging in the target at the heterogeneous tissue interfaces. Furthermore, the difficulties in modeling the fragmentation tail have been previously reported and might contribute to incorrect dose predictions for organs at risk (OAR)[27] located at the distal end of the beam.

The focus of this work was twofold: First, to benchmark pencil beam dose calculations for scanned carbon ion beams against measured dose distributions in heterogeneous phantom geometries for clinically relevant materials. Besides setups with different air gaps, setups with range shifter were studied for shallow target depths. Apart from the dose inside the target, also the distributions behind the target were analyzed to study the dose calculation accuracy for adjacent OARs and normal tissue, respectively. Secondly, the results for carbon ions were compared to PB and MC-based dose calculations for protons.

2 | MATERIALS AND METHODS

2.1 | Dose calculation algorithms and treatment planning

All dose calculations and treatment plan optimizations for scanned ion therapy were performed with the TPS RayStation (RaySearch Laboratories, Sweden). The carbon ion delivery sequences were optimized to achieve a uniform physical target dose. The dose calculations used the pencil beam algorithm (PB v3 in RayStation v7.99) which is at present the only available algorithm for carbon ions in the RayStation TPS. The dose contribution from each beamlet is calculated by performing a convolution of the lateral dose profile with the dose kernel for the subspot. The PB model-based dose calculations for carbon ions are labeled as "carbon PB" in the following.

Proton data from a previous study[28] were partly reused and added to this study to facilitate the comparison between the different dose calculations in proton

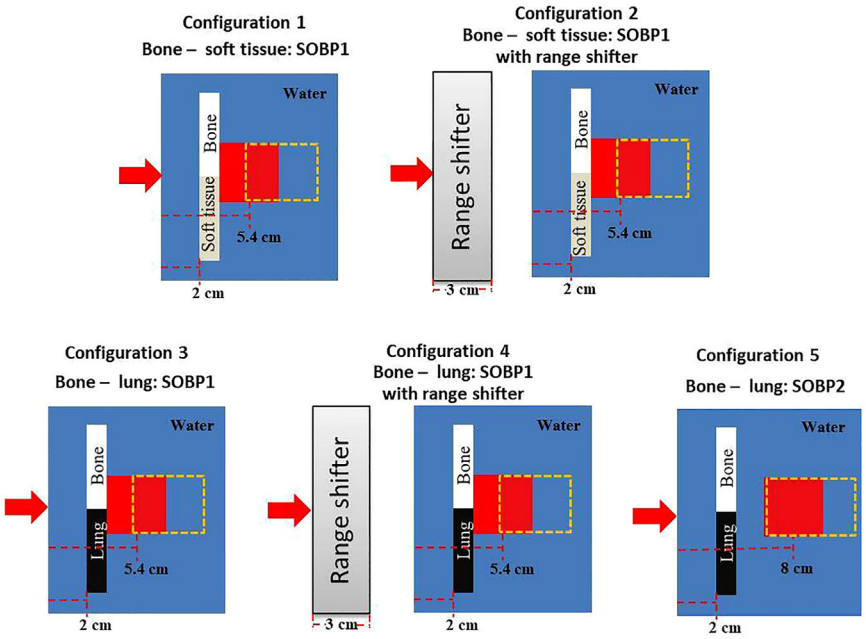

FIGURE 1 Overview of setup configurations. The solid red rectangles represent the target; the dashed rectangles indicate the region where the IC array was positioned. Configuration 1: target directly behind bone and soft tissue inserts (SOBP1). Configuration 2: target directly behind bone and soft tissue inserts (SOBP1) with presence of a range shifter. Configuration 3: target directly behind bone and lung inserts (SOBP1). Configuration 4: target directly behind the bone and lung inserts (SOBP1) with presence of a range shifter. Configuration 5: target at 8 cm from the inner surface of the water phantom behind bone and lung inserts (SOBP2)

TABLE 1 Overview of all test cases used in this study

Test case (configuration)	Material inserts	Target	Range shifter	Air gap (cm)	Particle type and energy range	
					Carbons (MeV/n)	Protons (MeV)
1 (1)	Bone–Soft tissue	SOBP1	–	16.1	127.0– 209.4	–
2 (2)	Bone–Soft tissue	SOBP1	in	16.1	181.7–255.3	97.4–134.4
3 (1)	Bone–Soft tissue	SOBP1	–	36.1	127.0–209.4	67.5–112.3
4 (2)	Bone–Soft tissue	SOBP1	in	36.1	181.7–255.3	97.4–134.4
5 (1)	Bone–Soft tissue	SOBP1	–	66.1	127.0–209.4	67.5–109.6
6 (3)	Bone–Lung	SOBP1	–	16.1	120.0–209.4	–
7 (4)	Bone–Lung	SOBP1	in	16.1	168.4–253.0	–
8 (3)	Bone–Lung	SOBP1	–	66.1	120.0–209.4	62.4–109.6
9 (4)	Bone–Lung	SOBP1	in	66.1	168.4–253.0	–
10 (5)	Bone–Lung	SOBP2	–	66.1	154.3–242.3	83.9–129.0

and carbon ion therapy. Dose distributions for protons were calculated in RayStation using the MC optimization (v4.1 in RayStation v6.99) for spot positions and spot weights. Subsequently to MC-based optimization, dose distributions were calculated either with the MC algorithm (v4.1, labeled as proton MC) or PB algorithm (v4.2, labeled as proton PB).

Active modulation method is applied to generate spread-out Bragg peak (SOBP) at MedAustron (Center for Ion Therapy and Research), where the beam energies are varied via a synchrotron-based accelerator. Basic beam data acquisition and commissioning of the respective beam models for proton and carbon ions were performed as required by the vendor.[29] Identical setups were used for both particle beams, except for the fact that the carbon ion beam model was created with ripple filters, consisting of two 2-mm thick plates with a triangular structure made of Polymethyl Methacrylate (PMMA)[30] which were inserted in the nozzle. Accordingly, all measurements for carbon ions were performed with the ripple filters. At the commissioning stage a final agreement of 1.5% and 3% was obtained for carbon ions and proton beams, respectively.

2.2 | Test cases

The dose calculation accuracy of the TPS was evaluated by a comparison with dose distributions measured with ionisation chambers (IC) in five test configurations and 10 test cases (Figure 1, Table 1). Experimental setup was similar to the one described in a previous study for proton beams,[28] and therefore only brief summary is given: A CT model dataset of a water phantom with

inhomogeneities was generated in Matlab (2016b, Mathworks, USA) and imported into the TPS. The dimensions of the virtual water phantom were $50 \times 50 \times 50$ cm^3, and both voxel size and slice thickness were 1 mm. Inside the phantom various heterogeneities, that is, bone, lung, and soft tissue materials were positioned. These inhomogeneities, consisting of 1-cm thick slabs, were enclosed in a thin PMMA holder and surrounded by water. That way, energy losses and scattering for all materials were handled in the TPS.

A fixed target size of $4 \times 4 \times 4$ cm^3 was used, and dose calculations were performed for a grid size of $1 \times 1 \times 1$ mm^3. A physical target dose of 1 Gy was planned, that is, radiobiological models were not considered in this study. Two different SOBP scenarios with the SOBP located at two different depths behind the heterogeneous interfaces were considered: SOBP1 (starting directly behind the tissue interface) and SOBP2 (starting at 2.6-cm distance behind the heterogeneities).

The impact of the air gap was validated by changing the distance between the water phantom and the nozzle. For the isocentric setup, this distance was 66.1 cm. Besides the isocentric setup, two additional air gap settings of 36.1 cm and 16.1 cm were investigated for carbon ions, and these are categorized as non-isocentric setups. Additionally, a range shifter (PMMA) with a water-equivalent thickness of 3 cm was inserted in the beam path to investigate its influence on the dose calculation accuracy.

Figure 1 and Table 1 provide an overview of five configurations that make up the 10 test cases studied, including different air gaps. In summary, the following characteristics and parameters influencing the dose distribution were investigated:

1. The combination of different tissue-equivalent materials as heterogeneities.
2. The position of the target of $4 \times 4 \times 4$ cm^3 behind the heterogeneities (proximal and distal target).
3. The size of the air gap between the nozzle and the phantom (isocentric/non-isocentric setup).
4. The presence/absence of a range shifter.

Although using large air gaps in combination with range shifter does not represent clinical practice, the test case with the range shifter and largest air gap was investigated for bone–lung materials (test case 9) as a worst-case scenario.

2.3 | Experimental setup and dosimetric validation

All dosimetric experiments were carried out at MedAustron facility for proton and carbon ion therapy and based on the current standard patient-specific quality assurance (PS-QA) procedure.[31] The setup for absorbed dose measurements (shown in Figure 2) consisted of a water phantom (MP3-PL, PTW, Germany) with embedded heterogeneities: bone, lung, and soft tissue (CIRS, USA) and an array of 24 PinPoint ionization chambers (ICs, T31015, PTW, Germany) connected to two Multidos electrometers (T10004, PTW). All 24 ICs were placed in a 3D holder, made of PMMA, which was attached to the moving mechanism of the water phantom. The chambers in the 3D holder were aligned on a 6×4 grid. The spacing between the chambers in the holder was 12 mm (in depth) and 10 mm (laterally), and to obtain a higher measurement resolution the holder with ICs was moved in the horizontal plane on a grid of 6 mm (in depth) and 5 mm (laterally). The chamber arrangement and distances in the 3D block were specifically designed in such a way to avoid dose distortion effects.[32] In-house developed software (PS-QA script and PlanVerificator v1.1)[21,33] was used for IC array positioning as well as for comparing TPS calculated and measured doses. In this procedure, the effective point of measurement was accounted for at the respective IC positions. As recommended by IAEA TRS 398,[34] the reference point of every ionization chamber was positioned at the distance of $0.75 \times r_{cyl}$ further away from the phantom surface than the center of IC, hence, 0.75 mm.

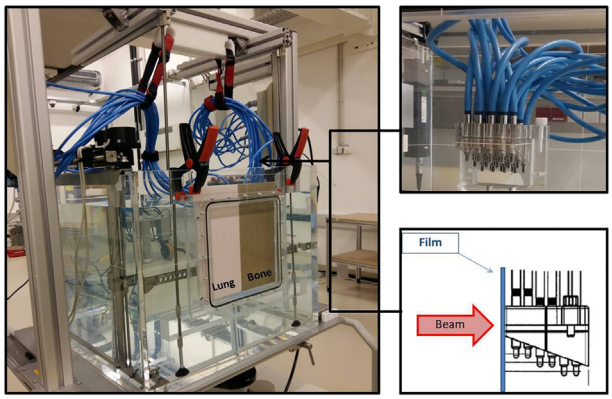

FIGURE 2 Experimental setup of the water phantom MP3-PL with inhomogeneous tissues (lung – bone tissue) and 24 ionization chambers. Upper right insert: 24 ICs in the 3D block. Lower right insert: EBT3 films attached to the front of the 3D holder for chambers (red arrow indicates the direction of the beam)

The focus of this study was on dose distributions along the interface region of two materials. The areas outside the target in lateral direction were not investigated. As illustrated in Figure 1, the region of interest (defined by the IC array) was positioned in the target volume and up to 3 cm behind the target.

In addition to IC measurements, radiochromic films (GafChromic EBT3, Ashland, KY, USA) were used for relative dosimetry to assess the lateral dose distributions at the distal part of the target for the test cased with and without the range shifter at the air gap of 16.1 cm (test case1, test case 2). For that purpose, the

TABLE 2 Summary of dose differences between calculations and IC measurements at regions of interest inside the target for all test cases

				Inside the target					
				Mean dose difference ± SD (%)			Maximum dose difference (%)		
				Carbon(*)	Proton[28]		Carbon(*)	Proton[28]	
Test case	Target	Range shifter	Air gap (cm)	PB	PB	MC	PB	PB	MC
Bone–soft tissue									
1	SOBP1	-	16.1	0.7 ± 0.6 (2.7 ± 4.5)	-	-	2.4 (15.0)	-	-
2	SOBP1	in	16.1	1.8 ± 1.0 (2.2 ± 1.7)	2.1 ± 1.4	2.0 ± 1.8	3.7 (8.0)	6.6	7.5
3	SOBP1	-	36.1	0.9 ± 0.7 (1.9 ± 2.6)	1.3 ± 1.5	1.2 ± 1.2	3.2 (11.1)	8.4	6.4
4	SOBP1	in	36.1	2.9 ± 1.2 (2.8 ± 1.2)	2.1 ± 1.9	2.0 ± 1.2	5.5 (5.5)	7.1	4.9
5	SOBP1	-	66.1	0.8 ± 0.5 (0.8 ± 0.7)	1.3 ± 1.1	1.2 ± 0.9	2.0 (3.7)	5.3	3.1
Bone–lung									
6	SOBP1	-	16.1	1.0 ± 0.6 (2.7 ± 4.1)	-	-	2.5 (15.3)	-	-
7	SOBP1	in	16.1	1.9 ± 1.0 (4.0 ± 5.4)	-	-	3.9 (24.6)	-	-
8	SOBP1	-	66.1	1.0 ± 0.5 (1.4 ± 1.5)	1.6 ± 1.2	1.1 ± 0.9	2.2 (8.1)	5.7	3.5
9	SOBP1	in	66.1	4.5 ± 1.4 (5.4 ± 3.3)	-	-	7.1 (20.5)	-	-
10	SOBP2	-	66.1	0.9 ± 0.7 (0.9 ± 0.7)	0.9 ± 0.7	0.6 ± 0.4	2.6 (2.6)	4.4	1.6

Abbreviation: PB, pencil beam; MC, Monte Carlo.
(*)The mean dose differences and corresponding standard deviations of measurements which include the last row of measurements inside the target for carbon ion beams are given in brackets.

EBT3 films were attached to the anterior surface of the 3D holder for the PinPoint IC and aligned in a way to coincide with the depth of the last row of PinPoint IC inside the target. Assessment with films was performed in one session successively to chamber measurements for both carbon and proton experiments. All irradiated films were scanned between 24 and 48 h after the exposure using a flatted scanner (Epson Expression 11000XL, Epson America, CA, USA).[35] Calibration curves were determined for dose ranges of 0–10 Gy for protons with a nominal energy of 148.2 MeV and 0–2 Gy for carbon ions with a nominal energy per nucleon of 402.8 MeV. An in-house developed Matlab program and the VeriSoft software (PTW, Freiburg, Germany) were employed for film analysis.

2.4 | Data analysis

Relative dose differences between the TPS calculated and experimental doses were determined and dose difference maps were created, where individual voxels correspond to a single chamber position. The dose differences were normalized to the maximum value of the calculated target dose in the underlying treatment plan[28]:

$$\textit{Percentage dose difference} = \frac{\textit{TPS predicted dose} - \textit{Measured dose}}{\textit{Maximum TPS predicted target dose}} \times 100. \quad (1)$$

Besides the mean dose differences, also the maximum dose deviations were calculated. The analyzed regions of interest were separated for the group of IC chambers located inside and behind the target region; the corresponding mean and maximum dose differences were always stated for both areas. Dose calculation accuracy was compared to the clinically acceptable tolerance level of 3%, defined for the target volumes.[36] For the data acquired outside the target volume, an additional evaluation was performed, where the differences between the TPS predicted and measured doses were normalized to the average of the TPS calculated dose. Dose profiles were derived from the irradiated EBT3 films at the distal edge of the target and compared with the TPS predicted dose distributions using a 1D gamma evaluation (gamma pass criteria 2% and 2 mm).

3 | RESULTS

Tables 2 and 3 summarize the results (percentage of the mean dose differences including respective standard deviations and maximum dose differences) inside and outside the target volume for both carbon ion and proton beams normalized to maximum TPS target dose. Inside the target, the mean and maximum dose differences between calculations and measurements for carbons ions, averaged over all the investigated test cases, were 1.6% and 3.5%, respectively. The results obtained outside the target area normalized to maximum value of the calculated target dose were 1.8% and 13.4%, respectively. Table 3 also provides an overview of the

TABLE 3 Summary of dose differences between calculations and IC measurements at regions of interest *behind the target* for all test cases

				Outside the target					
				Mean dose difference ± SD (%)			Maximum dose difference (%)		
Test case	Target	Range shifter	Air gap (cm)	Carbon(**)	Proton[28](**)		Carbon(**)	Proton[28](**)	
				PB	PB	MC	PB	PB	MC
Bone–soft tissue									
1	SOBP1	-	16.1	0.8 ± 2.4 (1.6 ± 5.0)	-	-	15.4 (31.7)	-	-
2	SOBP1	in	16.1	1.5 ± 2.0 (2.8 ± 3.7)	0.9 ± 1.3 (1.7 ± 2.5)	0.9 ± 1.5 (1.7 ± 2.8)	12.5 (23.2)	5.3 (9.9)	6.6 (12.6)
3	SOBP1	-	36.1	0.9 ± 2.2 (1.8 ± 4.4)	1.1 ± 2.3 (2.1 ± 4.5)	0.8 ± 1.6 (1.6 ± 3.2)	12.2 (24.8)	13.1 (25.6)	7.0 (13.9)
4	SOBP1	in	36.1	2.1 ± 1.5 (3.8 ± 2.8)	1.9 ± 3.0 (3.6 ± 5.7)	1.5 ± 2.4 (2.8 ± 4.5)	9.1 (16.6)	12.7 (12.7)	8.2 (15.2)
5	SOBP1	-	66.1	1.1 ± 2.4 (2.4 ± 5.0)	1.1 ± 2.5 (2.3 ± 5.0)	0.6 ± 1.2 (1.7 ± 3.6)	14.7 (30.7)	10.4 (21.2)	4.9 (8.9)
Bone–lung									
6	SOBP1	-	16.1	1.4 ± 3.4 (2.9 ± 6.8)	-	-	15.9 (31.6)	-	-
7	SOBP1	in	16.1	2.0 ± 3.7 (3.8 ± 7.3)	-	-	17.4 (34.0)	-	-
8	SOBP1	-	66.1	1.0 ± 1.7 (2.0 ± 3.5)	2.4 ± 4.1 (4.7 ± 8.2)	0.9 ± 1.5 (1.8 ± 2.9)	8.1 (16.1)	18.8 (37.6)	5.5 (10.9)
9	SOBP1	in	66.1	4.5 ± 3.1 (8.5 ± 5.9)	-	-	16.5 (31.2)	-	
10	SOBP2	-	66.1	2.6 ± 3.1 (3.8 ± 4.6)	2.4 ± 2.6 (3.7 ± 4.1)	1.2 ± 1.2 (2.0 ± 1.8)	12.0 (17.4)	12.1 (16.0)	4.1 (5.8)

Abbreviations: PB, pencil beam; MC, Monte Carlo; SOBP, spread-out Bragg peak.
(**)The mean dose differences normalized to averaged treatment planning system (TPS)-predicted dose and corresponding standard deviations of measurements are given in brackets.

data outside the target normalized to averaged calculated dose from TPS, with the mean dose difference of 3.3% and maximum dose difference of 24%.

The following sub-sections provide additional details on the comparison between carbon ion and proton dose calculations, presented for individual test cases which were investigated for both particle types (test cases 2-5, 8, 10). Due to the finite size of PinPoint IC, the data presented for carbon ions do not include the measurement points and corresponding calculations for the last measurement row in the target. Relative dosimetry at the distal fall-off region of the target (air gap of 16.1 cm, test case 1) was performed in addition to PinPoint IC also with Gafchromic EBT3 films. More details concerning the IC limitation are given in supplementary material, and the gamma distributions derived from EBT3 film measurements are shown in Figure S6.

3.1 | Impact of heterogeneous structures (bone–soft tissue vs. bone–lung)

For the bone–soft tissue interface and the region of interest located within the target volume (test cases 3 and 5), the mean dose differences were 0.9% for the carbon PB algorithm and 1.3%/1.2% for proton PB/MC, respectively. For the bone–lung interface (test case 8 and 10), the differences were very similar for all algorithms, that is, 1.0% for carbon PB, 1.3% for proton PB, and 0.9% for proton MC.

Comparing the dose distributions behind the target, on average larger local dose differences were observed for the proton PB algorithm when compared to carbon PB results. For the bone–soft tissue interface (test case 3 and 5), the respective values were the same for both proton and carbon ion PB calculations (1.1%), while the best agreement (0.6%) was obtained for the proton MC algorithm. The largest local dose difference of +14.7% for the carbon ion PB was found directly at the interface region between bone and soft tissue but corresponded only to one measurement point. The discrepancy extended further behind the target for the bone–lung tissue configuration covering typically three measurement points (Figures 3a and 5d). For proton PB calculations, the largest local dose underestimation of up to −18.8% was obtained behind the bone–lung interface.

Figure 3 shows the dose distributions calculated by the TPS, as well as the percentage difference between the calculated and experimentally determined dose values for the bone–lung interface (Test case 8) for all three algorithms. The size of the discrepancy region was significantly larger for proton PB compared to carbon ions (Figure 3b). The mean dose differences for the bone–lung interface (test case 8 and 10) were 1.8% for carbon PB and 2.4%/1.1% for proton PB/MC, respectively. The local dose differences for carbon ions for the bone–lung interface reached up to 8.1%, covering about three measurement points (Figure 3a). As expected, the best results were obtained for proton MC with maximum dose difference of 4.9%/4.1% behind the bone–soft/bone–lung tissue interfaces.

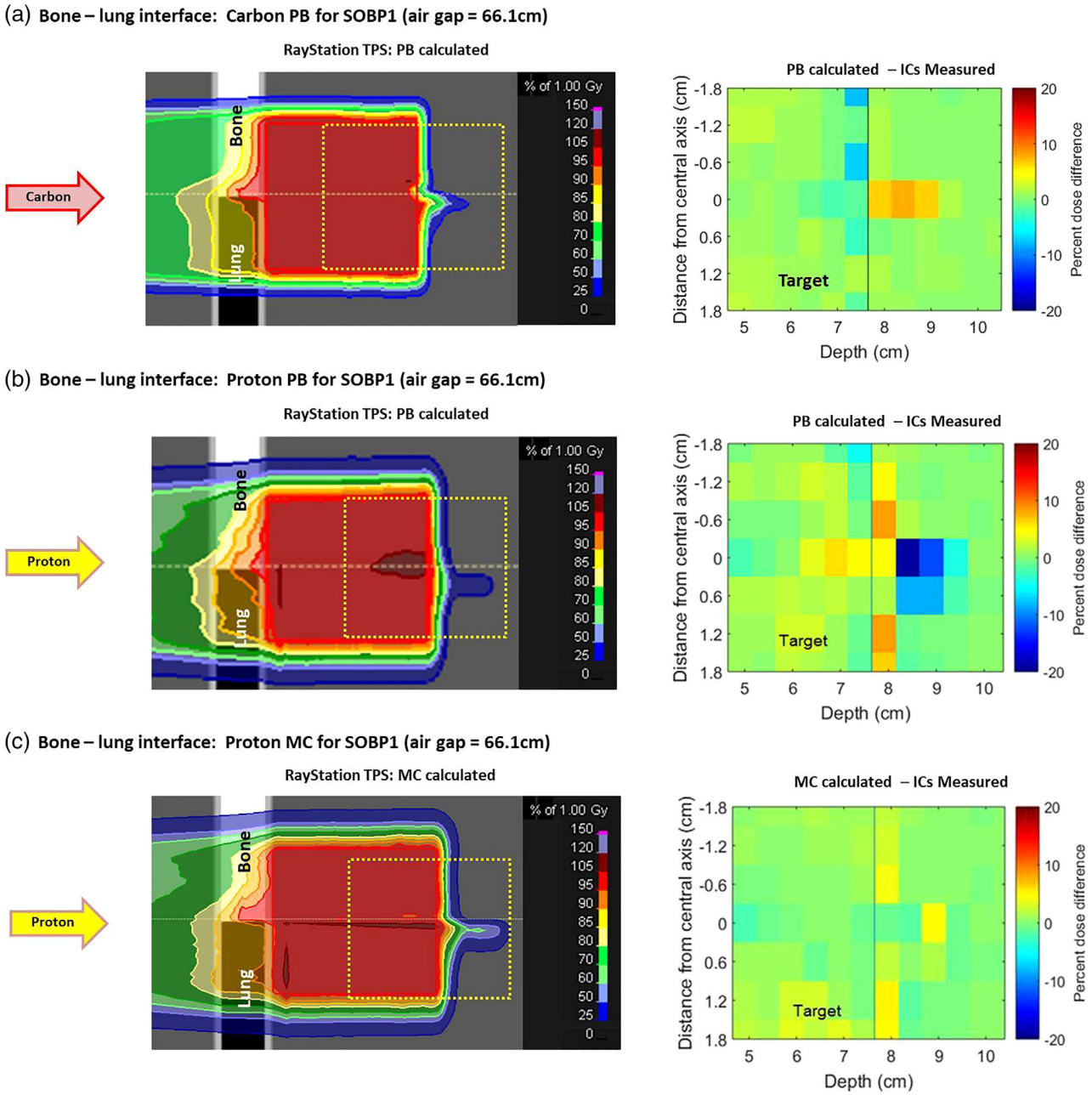

FIGURE 3 Dose distribution analysis for test case 8 at the bone–lung interface: Treatment planning system (TPS) calculated doses are shown in the left column. Dose difference maps between the planned and measured dose are shown in the right column; (a) carbon PB; (b) proton PB; (c) proton MC. The yellow dashed squares (left column) indicate the measurement region. The black vertical lines in the right column indicate the border between the target region and the region beyond the target. The blue color code indicates a dose underestimation by the TPS, red/orange an overestimation. The right panel of row (b) and (c) in the figure are reproduced with permission from[28]

3.2 | Impact of target depth (proximal: SOBP1 vs. distal target: SOBP2)

Figure 4 shows the histograms of the dose differences for both targets for carbon ion and proton dose calculations at the isocentre (test case 8 and 10). For the carbon ion PB algorithm, no systematic differences could be observed for measurement points located within the target for the two depths, that is, mean and maximum dose differences were about 1.0% and 2.4%. For the proton PB algorithm results were slightly worse for SOBP1 compared to SOBP2, with mean and maximum dose differences of 1.6% and 5.7% (SOBP1) compared to 0.9% and 4.4% for SOBP2.

The largest dose differences outside the target reached 8.1% for carbon ions in SOBP1 and 12.0% for SOBP2, with an overestimated dose by the TPS. On the contrary, for protons, the dose was underestimated, especially for SOBP2 with maximum local differences of up to 12.1%. The performance of the proton

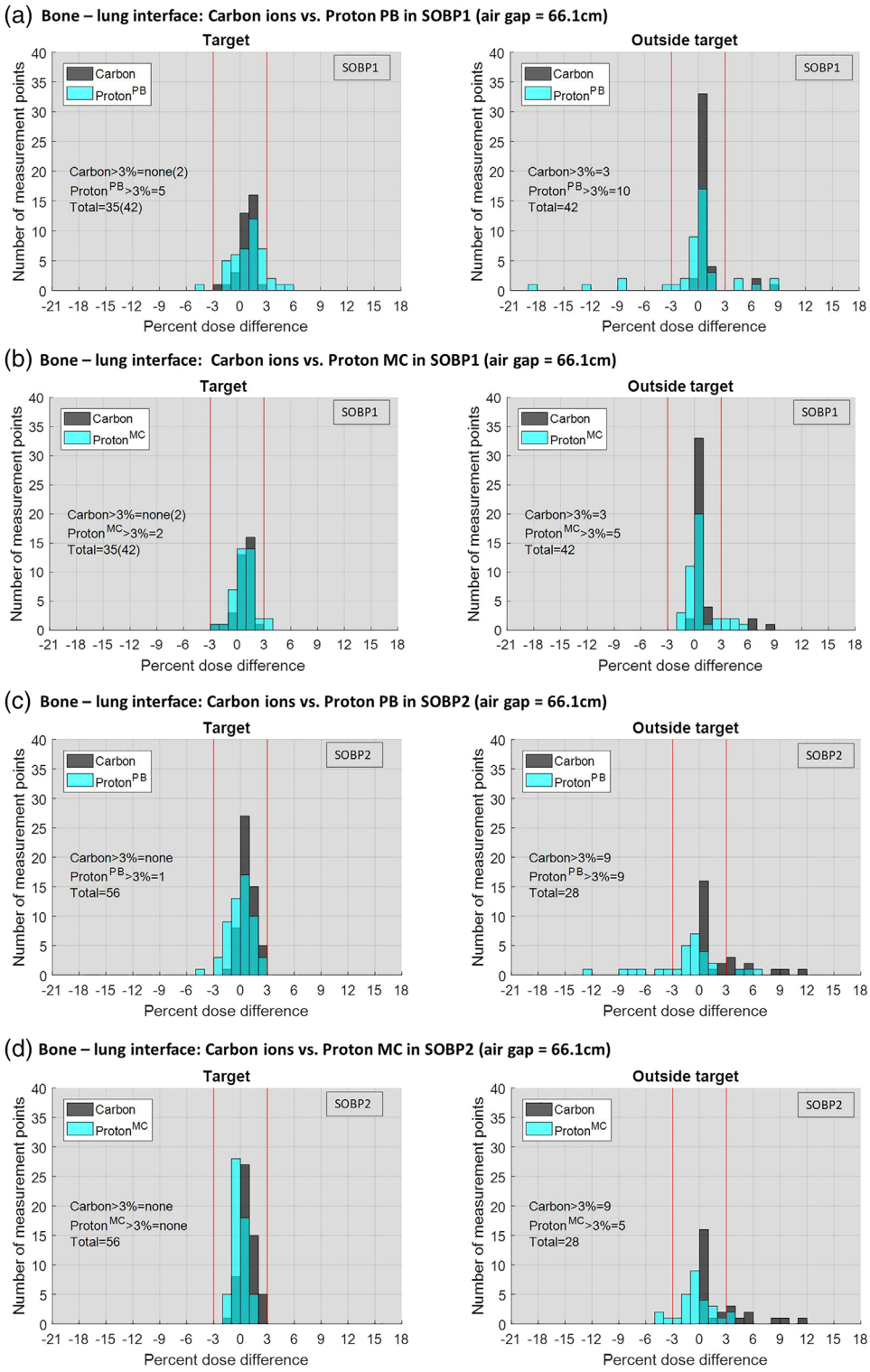

FIGURE 4 Histograms of dose differences between the calculations and measurements for carbon ions and proton beams for the bone–lung interface (no range shifter); (a) carbon ion and proton PB SOBP1 (test case 8); (b) carbon ion and proton MC SOBP1 (test case 8); (c) carbon ion and proton PB SOBP2 (test case 10) and (d) carbon ion and carbon ion versus proton MC SOBP2 (test case 10). Red vertical lines indicate an acceptable interval (within 3%)

MC algorithm was best, with a slight dose overestimation for SOBP1 but an underestimation for SOBP2 inside and outside the target. In general, better agreement between calculations and measurements were obtained for SOBP2.

3.3 | Impact of air gap between nozzle and phantom

The performance of dose calculations was comparable for all test cases without the range shifter, for all three investigated air gaps (test cases 3, 5, 8, 10). The averaged mean dose difference for carbon ions inside/outside the target was 0.8% /1.4%. The averaged mean dose difference inside and outside the target for proton PB/MC was 1.2%/1% and 1.3%/0.9%, respectively. A similar trend as in previous test cases (section 3.2), that is, an overestimation of the calculated dose for carbon ions and an underestimation for proton PB, was also observed behind the target for these test cases.

The dose distributions for both the carbon ion PB and the proton PB algorithm for the setup configuration with the bone–soft tissue slabs at the air gap of 36.1 cm (Test case 3) are shown in Figure S1a,b. The performance of the carbon ion PB algorithm was slightly better than for the proton PB algorithm, both inside and outside the target volume. The results from carbon ion PB dose calculations for the setups with the bone–soft tissue and bone–lung at the air gap of 16.1 cm (test case 1 and 6) are illustrated in supplementary material (Figure S1c,d). These test cases were available only for carbon ion beams. The agreement between the calculations and measurements was better for the bone–soft tissue interface than for the bone–lung tissue interface; however, these differences were rather small for points of interest located inside the target.

Although acceptable dosimetric agreement was found for carbon ion PB calculations within the target for the isocentric setups (test cases 5, 8, 9, 10), smaller air gaps led to large dose deviations at the last measurement row in the target (Figure S1). The local differences were largest for the smallest investigated air gap of 16.1 cm (test case 1 and 6). The agreement between dose calculations and IC measurements at the end of the target improved with decreasing density of the inhomogeneities and with increasing air gap. However, clinically unacceptable dosimetric differences of more than 3% were found for the air gap of 36.1 cm along the last measurement row. The different behavior of carbon ion and proton dose calculation as a function of air gaps might be related to the generally broader Bragg peaks as well as the broader distal fall-off of the SOBP in protons. A possible explanation for these differences at the last measurement row might be positioning uncertainties of the IC chambers. Therefore, measurements for the last row of the IC and the corresponding TPS calculations were excluded from all the test cases for carbon ions, that is, measurement results referring to last IC array row are listed in brackets in Table 2. More on the potential limitation of PinPoint IC at the distal fall-off is given in supplementary material.

3.4 | Impact of a range shifter

The range shifter, modeled as a passive external element in the TPS RayStation, was tested in combination with three different air gaps only for carbon ions. The average dose differences between TPS calculations and measurements for all investigated air gaps with range shifter (test cases 2, 4, 7, 9), inside and outside the target, were larger than 1.5%. The performance of the carbon PB dose calculation was getting gradually worse with increasing air gap. The mean dose differences in the target were 1.8% (air gap 16.1 cm, test case 2) and 2.9% (air gap 36.1 cm, test case 4) which was within the clinically acceptable interval (±3%) for the non-isocentric setups (see Figurs S2 and S3). The largest discrepancies were observed at the isocenter for the bone–lung setup (test case 9), where the carbon ion dose calculations overestimated the dose in most of the target, with mean dose difference of 4.5% and maximum differences of more than 7%. The histograms of the deviations between the calculated and measured dose values for carbon ions (bone–lung tissues) at 16.1 cm and 66.1 cm air gaps are shown in Figure 5, the respective dose distributions for these test cases are shown in Figure S4. The number of measurement points exceeding the clinically acceptable level of 3% was 32 of 38. The mean dose difference outside the target volume was 4.5% (the same as inside the target), and the maximum local differences were up to 16.5%.

Comparing results for the carbon ion PB algorithm with and without range shifter for the air gap of 36.1 cm, better agreement was achieved for measurements without the range shifter (Figure S5). The mean dose differences inside the target with and without the range shifter were 2.9% and 0.9%, respectively.

4 | DISCUSSION

Protons and carbon ions are the two particle species currently applied in clinical studies. While the number of proton centers is rapidly increasing at the global level, carbon ion therapy is developing at a much lower pace.[37,38] A direct comparison between the dose calculation accuracy of proton beams and carbon ion beams has not been performed so far but is generally desirable for example, to rule out systematic dosimetric differences and to assure that the dosimetry of both modalities is of similar quality when exploring their clinical benefits. Proton beams have been investigated

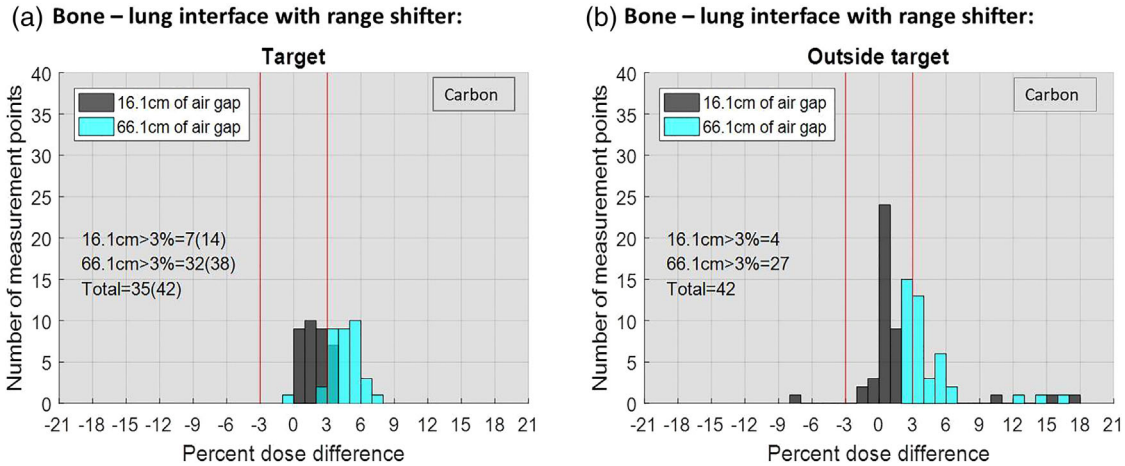

FIGURE 5 Histograms of dose differences in carbon ions between the calculations and measurements with the range shifter for the air gaps of 16.1 cm (test case 7) and 66.1 cm (test case 9) for the bone–lung interface; (a) inside the target and (b) Outside the target. Red vertical lines indicate an acceptable interval ± 3%

by several groups covering all currently available commercial TPSs. Existing literature typically focuses on dose distributions in target areas, while dose reporting outside the target is rather limited.[17,39] Differently to protons, literature that reports on the accuracy of commercial dose calculations for carbon ion therapy with PB scanning is scarce.

In this work, we benchmark a current state of the art analytical dose calculation algorithm for carbon ion beams against the dosimetric measurements in various complex test cases that are relevant for clinical scenarios. The proton results discussed in this study were obtained in a previous study.[28] Using the same setup and test cases to validate carbon ion dose calculations provides the advantage of enabling a direct comparison.

For the carbon ion measurements in the heterogeneous setup, mean dose differences between calculations and measurements at points of interest inside the target were of the same order of magnitude as commissioning results in water. The mean dose difference and maximum dose differences outside the target area were higher and the latter exceeded 10% for the majority of measurements.

As expected, the largest dosimetric difference was observed along the interface of two tissue materials bone–soft tissue and/or the bone–lung. For the PB proton algorithm a higher accuracy was obtained for the bone–soft tissue interfaces which can be understood by the smaller density variation relative to the bone–lung test case. Similar general findings were reported for realistic animal tissue phantoms.[40] For protons, a reduced sensitivity with respect to different tissues was previously shown in a MC study.[17] In the current study, the proton MC was less sensitive to tissue variations as proton PB. The carbon ion PB performed within the target as good as proton MC.

Comparing the two heterogeneous interfaces for carbon ions, a "dose discrepancy tail" was observed for all configurations with the bone–lung interface. This might be related to difficulties to model the production of nuclear fragments and their momentums for tissues with larger material densities. On the other hand, despite the difficulties to accurately model the fragmentation tail for carbon ions, the volume of local discrepancies was larger for the proton PB algorithm. This is to be expected because the angular distribution of carbon ions is narrow. The proton fragments, even though they have a longer range, are still narrower than the primary proton scattering in the proton fields. Dose deviations behind the target for carbon ions in the bone–soft tissue configuration was typically limited to one measurement point, whereas for bone–lung tissues it reached up to three measurement points, corresponding to 1.5 cm wide regions. These regions reached up to 2 cm for PB proton calculations and extended laterally, especially for the test cases with bone–lung interface. Range struggling depends on material uniformity, and as reported in a recent proton study, different lung substituting materials led to different range uncertainties.[41] Carbon ion calculations had a tendency of over predicting and proton PB under predicting the doses to healthy tissues. Comparing all three algorithms, the best performance behind the target was achieved for the proton MC algorithm for which also the size of local discrepancies was the smallest.

In this study, the mean dose difference for a test case represents the average deviation from all IC measurement points inside or outside the target. Thus, it is important to note that more complex test geometries, for example, with more tissue interfaces, will potentially lead to larger mean dose differences. The level of complexity as well as evaluation method (relative to maximum or averaged TPS target dose or local

dose) should be therefore considered when comparing published results. Compared to advanced photon beam therapy, there are no standardized phantoms or test geometries for TPS commissioning or end-to-end test in particle therapy.[42,43] Other factors, for example, dose grid resolution, will also have an impact on the dose calculation accuracy, that is, a lower resolution will lead to larger deviations, especially at the interfaces of different materials.

Several studies reported on a systematic overestimation of target doses by about 1%–2%[44] or even more[18,45] for analytical dose calculations, irrespective of TPS, which is in line with our findings from PB calculations, for both protons and carbon ions. This overestimation was more pronounced for larger air gaps in combination with the range shifter.

Comparing two target depths and dose distributions behind the target for carbon ions, the dose discrepancies are larger for the distal target (SOBP2). Carbon ions traversing matter are significantly affected by nuclear fragmentation leading to primary beam attenuation and increased build-up of fragments and could explain the differences between the measured and calculated doses for carbon ions in this work. As previously reported, the modeling is more challenging with increasing penetration depth.[2,46]

A slight and systematic dose overestimation was also observed for the shallow target (SOBP1) without the range shifter for the proton MC algorithm. These results are in line with the findings of others, who reported a 1%–2% agreement between measurements clinical MC dose calculations implemented in commercial TPS.[47,48] Aitkenhead et al.[48] reported that any of such results might be affected by the test case, that is, phantom material, degree of field modulation, or detector used.

Looking at the local variations across the target, which were averaged over six test cases available for all three algorithms, the best agreement was obtained for carbon beams (3.2%) followed by proton MC (4.5%) and proton PB (6.3%), indicating that the most homogeneous target dose distributions in the presence of inhomogeneities was achieved with carbon ion beams.

For the TPS RayStation's PB algorithm, there is no explicit modeling of the nuclear halo broadening in the air gap between the range shifter and the patient. For large air gaps, this can lead to an underestimation of the lateral dose. This is a well-known limitation of the PB algorithms, as secondary particles, the particle transport over the air gaps and the halo created in the range shifter are not properly handled.[21,25,28] The results obtained for carbon ions performed in the heterogeneous phantom confirm these findings. Carbon ion results using the range shifter were systematically worse compare to the test cases without the range shifter, even for the smallest air gap of 16.1 cm, and the dose deviations were increasing with larger air gaps. The clinically unacceptable dose over prediction of 4.5% (mean dose difference) was obtained for the test case with bone–lung tissue at the isocenter. The number of measurement points exceeding the clinically acceptable level of 3% was 32 of 38, leading to the conclusion that the dose cannot be predicted with sufficient accuracy by the PB dose algorithm for the large air gaps with the range shifter. Therefore, this configuration is not recommended for clinical treatments and underlines the necessity for MC-based calculations for carbon ions to use the modality to its full potential. The use of MC dose calculations for clinical treatment planning with carbon ions is not a conventional practice yet, mainly due to remaining uncertainties in the cross-section data for clinically relevant energy range and long computation times.[49]

5 | CONCLUSION

PB dose calculations for carbon ions in complex test cases were in a good agreement with dosimetric measurements for all points of interest located inside the target volume except the test cases with range shifter. The performance of the PB algorithm for carbon ions was better than the PB dose algorithm for protons. Larger local dose differences between the calculations and measurements were observed for points of interest behind the target, especially for tissue interfaces with very large density gradients, such as bone–lung tissues. For points of interest behind the target area, a systematic overestimation of the local dose was observed for carbon ion beams, which might affect DVH calculations and clinical results in the worst case.

ACKNOWLEDGMENTS

Author Sirinya Ruangchan gratefully acknowledges the financial support by PhD research grant from the Thai Red Cross Society, King Chulalongkorn Memorial Hospital, Bangkok.

CONFLICT OF INTEREST

The authors have no conflict to disclose.

DATA AVAILABILITY STATEMENT

The data that support the findings of this study are available from the corresponding author upon reasonable request.

REFERENCES

1. Particle Therapy Co-Operative Group (PTCOG). Particle therapy facilities in clinical operation (last update: August 2021). www.ptcog.ch/index.php/facilities-in-operation. Accessed March 19, 2021.
2. Haettner E, Iwase H, Krämer M, Kraft G, Schardt D. Experimental study of nuclear fragmentation of 200 and 400 MeV/u 12C ions in water for applications in particle therapy. *Phys Med Biol*. 2013;58(23):8265-8279.
3. Resch AF, Fuchs H, Georg D. Benchmarking GATE/Geant4 for 16O ion beam therapy. *Phys Med Biol*. 2017;62(18):N474-N484.

4. Jäkel O. Physical advantages of particles: protons and light ions. *Br J Radiol*. 2020;93(1107):20190428.
5. Dreher C, Combs SE. Clinical rationale and indications for particle therapy. *Progress in Tumor Research*. S. Karger; 2018:89-104.
6. Tinganelli W, Durante M. Carbon ion radiobiology. *Cancers*. 2020;12:(10):3022. https://doi.org/10.3390/cancers12103022
7. Kamada T, Tsujii H, Blakely EA, et al. Carbon ion radiotherapy in Japan: an assessment of 20 years of clinical experience. *Lancet Oncol*. 2015;16(2):e93-e100.
8. Eason L, Mason J, Cooper R, Radhakrishna G, Bownes P. Evaluation of a collapsed-cone convolution algorithm for esophagus and surface mold 192Ir brachytherapy treatment planning. *Brachytherapy*. 2020;20(2):393-400.
9. Beaulieu L, Carlsson Tedgren Å, Carrier JF, et al. Report of the Task Group 186 on model-based dose calculation methods in brachytherapy beyond the TG-43 formalism: current status and recommendations for clinical implementation. *Med Phys*. 2012;39(10):6208-36.
10. Ma Y, Lacroix F, Lavallée MC, Beaulieu L. Validation of the oncentra brachy advanced collapsed cone engine for a commercial 192Ir source using heterogeneous geometries. *Brachytherapy*. 2015;14(6):939-52.
11. Kragl G, Albrich D, Georg D. Radiation therapy with unflattened photon beams: dosimetric accuracy of advanced dose calculation algorithms. *Radiother Oncol*. 2011;100(3):417-23.
12. Künzler T, Fotina I, Stock M, Georg D. Experimental verification of a commercial Monte Carlo-based dose calculation module for high-energy photon beams. *Phys Med Biol*. 2009;54(24):7363-7377.
13. Saini J, Traneus E, Maes D, et al. Advanced proton beam dosimetry part I: review and performance evaluation of dose calculation algorithms. *Transl Lung Cancer Res*. 2018;7(2):171-179.
14. Langner UW, Mundis M, Strauss D, Zhu M, Mossahebi S. A comparison of two pencil beam scanning treatment planning systems for proton therapy. *J Appl Clin Med Phys*. 2018;19(1):156-163.
15. Saini J, Traneus E, Maes D, et al. Advanced Proton Beam Dosimetry Part I: review and performance evaluation of dose calculation algorithms. *Transl Lung Cancer Res*. 2018;7(2):171-179.
16. Resch AF, Elia A, Fuchs H, et al. Evaluation of electromagnetic and nuclear scattering models in GATE/Geant4 for proton therapy. *Med Phys*. 2019;46(5): 2444–2456.
17. Maes D, Saini J, Zeng J, Rengan R, Wong T, Bowen SR. Advanced proton beam dosimetry part II: Monte Carlo vs. pencil beam-based planning for lung cancer. *Transl Lung Cancer Res*. 2018;7(2):114-121.
18. Taylor PA, Kry SF, Followill DS. Pencil beam algorithms are unsuitable for proton dose calculations in lung. *Int J Radiat Oncol*. 2017;99(3):750-756.
19. Sorriaux J, Testa M, Paganetti H, et al. Experimental assessment of proton dose calculation accuracy in inhomogeneous media. *Phys Medica*. 2017;38:10-15.
20. Ciangaru G, Polf JC, Bues M, Smith AR. Benchmarking analytical calculations of proton doses in heterogeneous matter. *Med Phys*. 2005;32(12):3511-3523.
21. Carlino A, Böhlen T, Vatnitsky S, et al. Commissioning of pencil beam and Monte Carlo dose engines for non-isocentric treatments in scanned proton beam therapy. *Phys Med Biol*. 2019;64(17):17NT01.
22. Beltran C, Tseung HWC, Augustine KE, et al. Clinical implementation of a proton dose verification system utilizing a GPU Accelerated Monte Carlo Engine. *Int J Part Ther*. 2016;3(2):312-319.
23. Vogin G, Wambersie A, Koto M, et al. A step towards international prospective trials in carbon ion radiotherapy: investigation of factors influencing dose distribution in the facilities in operation based on a case of skull base chordoma. *Radiat Oncol*. 2019;14(1):24.
24. Manual. *RayStation 7 Reference Manual*. Stockholm: RaySearch Laboratories AB; 2017.
25. Saini J, Maes D, Egan A, et al. Dosimetric evaluation of a commercial proton spot scanning Monte-Carlo dose algorithm: comparisons against measurements and simulations. *Phys Med Biol*. 2017;62(19):7659-7681.
26. Manual. *RayStation 8B Reference Manual*. Stockholm: RaySearch Laboratories AB; 2018.
27. Slater JM. *Ion Beam Therapy: Fundamentals, Technology, Clinical Applications*. Springer, Berlin, Heidelberg: Springer; 2012.
28. Ruangchan S, Knäusl B, Fuchs H, Georg D, Clausen M. Physica medica experimental benchmarking of RayStation proton dose calculation algorithms inside and outside the target region in heterogeneous phantom geometries. *Phys Medica*. 2020;76(July):182-193.
29. Manual. *Raystation 8B User Manual*. Stockholm: RaySearch Laboratories AB; 2018.
30. Grevillot L, Stock M, Vatnitsky S. Evaluation of beam delivery and ripple filter design for non-isocentric proton and carbon ion therapy. *Phys Med Biol*. 2015;60(20):7985-8005.
31. Stock M, Georg D, Ableitinger A, et al. The technological basis for adaptive ion beam therapy at MedAustron : status and outlook. *Zeitschrift fßr Medizinische Phys*. 2018;28(3):196-210.
32. Karger CP, Jäkel O, Hartmann GH, Heeg P. A system for three-dimensional dosimetric verification of treatment plans in intensity-modulated radiotherapy with heavy ions. *Med Phys*. 1999;26(10):2125-32.
33. Grevillot L, Stock M, Palmans H, et al. Implementation of dosimetry equipment and phantoms at the MedAustron light ion beam therapy facility. *Med Phys*. 2018;45(1):352-369.
34. INTERNATIONAL ATOMIC ENERGY AGENCY. *Implementation of the International Code of Practice on Dosimetry in Radiotherapy (TRS 398): Review of testing results*. Vienna: IAEA; 2005.
35. Khachonkham S, Dreindl R, Heilemann G, et al. Characteristic of EBT-XD and EBT3 radiochromic film dosimetry for photon and proton beams. *Phys Med Biol*. 2018;63(6):065007.
36. Miften M, Olch A, Mihailidis D, et al. Tolerance limits and methodologies for IMRT measurement-based verification QA: Recommendations of AAPM Task Group No. 218. *Med Phys*. 2018;45(4):e53-e83.
37. Jäkel O. Physical advantages of particles: protons and light ions. *Br J Radiol*. 2020;93(1107):20190428.
38. Dreher C, Combs SE. Clinical Rationale and Indications for Particle Therapy. *Prog Tumor Res*. 2018;44:89-104.
39. Jäkel O, Ackermann B, Ecker S, et al. Methodology paper: A novel phantom setup for commissioning of scanned ion beam delivery and TPS. *Radiat Oncol*. 2019;14(1):77.
40. Schreuder AN, Bridges DS, Rigsby L, et al. Validation of the RayStation Monte Carlo dose calculation algorithm using realistic animal tissue phantoms. *J Appl Clin Med Phys*. 2019;20(10):160-171.
41. Hranek A, Resch AF, Georg D, Knäusl B. Investigation of the Bragg peak degradation caused by homogeneous and heterogeneous lung tissue substitutes: proton beam experiments and comparison to current clinical dose calculation. *Phys Med Biol*. 2020.
42. Jamema S V., Upreti RR, Sharma S, Deshpande DD. Commissioning and comprehensive quality assurance of commercial 3D treatment planning system using IAEA technical report series — 430. *Australas Phys Eng Sci Med*. 2008;31(3):207-215.
43. Gershkevitsh E, Schmidt R, Velez G, et al. Dosimetric verification of radiotherapy treatment planning systems: results of IAEA pilot study. *Radiother Oncol*. 2008;89(3):338-346
44. Schuemann J, Giantsoudi D, Grassberger C, Moteabbed M, Min CH, Paganetti H. Assessing the clinical impact of approximations in analytical dose calculations for proton therapy. *Int J Radiat Oncol Biol Phys*. 2015;92(5):1157-1164.

45. Taylor PA, Kry SF, Alvarez P, et al. Results from the imaging and radiation oncology core Houston's anthropomorphic phantoms used for proton therapy clinical trial credentialing. *Int J Radiat Oncol Biol Phys*. 2016;95(1):242-248.
46. Hollmark M, Belkić D, Gudowska I, Brahme A. Influence of multiple scattering and energy loss straggling on the absorbed dose distributions of therapeutic light ion beams: I. Analytical pencil beam model. *Phys Med Biol*. 2004;49(14):3247-3265.
47. Lin L, Huang S, Kang M, et al. A benchmarking method to evaluate the accuracy of a commercial proton monte carlo pencil beam scanning treatment planning system. *J Appl Clin Med Phys*. 2017;18(2):44-49.
48. Aitkenhead AH, Sitch P, Richardson JC, Winterhalter C, Patel I, Mackay RI. Automated Monte-Carlo re-calculation of proton therapy plans using Geant4/Gate : implementation and comparison to plan-specific quality assurance measurements. *Br J Radiol*. 2020;93(1114):20200228.
49. Dedes G, Parodi K. Monte carlo simulations of particle interactions with tissue in carbon ion therapy. *Int J Part Ther*. 2015;2(3):447-458.
50. Resch AF, Heyes PD, Fuchs H, Bassler N, Georg D, Palmans H. Dose- rather than fluence-averaged LET should be used as a single-parameter descriptor of proton beam quality for radiochromic film dosimetry. *Med Phys*. 2020;47(5):2289-2299.
51. Gambarini G, Bettega D, Camoni G, et al. Development of a procedure for quenching-effect correction in images of absorbed dose from protons or carbon ions acquired with Gafchromic EBT3 films. *Radiat Phys Chem*. 2019;155:138-145.

SUPPORTING INFORMATION

Additional supporting information may be found in the online version of the article at the publisher's website.

How to cite this article: Ruangchan S, Palmans H, Knäusl B, Georg D, Clausen M. Dose calculation accuracy in particle therapy: Comparing carbon ions with protons. *Med Phys*. 2021;48:7333–7345.
https://doi.org/10.1002/mp.15209